

RIS-assisted Cell-Free MIMO with Dynamic Arrivals and Departures of Users: A Novel Network Stability Approach

Charbel Bou Chaaya¹, Mohamad Assaad² and Tijani Chahed¹

¹ *Institut Polytechnique de Paris, Telecom SudParis, 19 Place Marguerite Perey, 91120 Palaiseau, France*

² *University of Paris-Saclay, CNRS, CentraleSupélec, Laboratoire des signaux et systèmes, 91190 Gif-sur-Yvette, France*

Abstract—Reconfigurable Intelligent Surfaces (RIS) have recently emerged as a hot research topic, being widely advocated as a candidate technology for next generation wireless communications. These surfaces passively alter the behavior of propagation environments enhancing the performance of wireless communication systems. In this paper, we study the use of RIS in cell-free multiple-input multiple-output (MIMO) setting where distributed service antennas, called Access Points (APs), simultaneously serve the users in the network. While most existing works focus on the physical layer improvements RIS carry, less attention has been paid to the impact of dynamic arrivals and departures of the users. In such a case, ensuring the stability of the network is the main goal. For that, we propose an optimization framework of the phase shifts, for which we derived a low-complexity solution. We then provide a theoretical analysis of the network stability and show that our framework stabilizes the network whenever it is possible. We also prove that a low complexity solution of our framework stabilizes a guaranteed fraction (higher than 78.5%) of the stability region. We provide also numerical results that corroborate the theoretical claims.

Index Terms—Reconfigurable Intelligent Surfaces (RIS), Cell-free MIMO, Stability Region, Flow-level modeling, Dynamic user configuration

I. INTRODUCTION

UNPRECEDENTED communication requirements for Beyond 5G networks will call for essentially new schemes. Numerous technologies have been investigated in the last few decades to satisfy the exponential surge for wireless connectivity, notably massive Multiple-Input Multiple-Output (mMIMO) [1], [2], ultra dense networks (UDN) and millimeter waves (mmWave) [3]. The reliable service offered by these innovations however, comes at the cost of expensive hardware and high energy consumption. Consequently, extensive research is ongoing to find novel designs for sustainable wireless networks with spectrum and power efficiencies, and low hardware cost.

Reconfigurable intelligent surfaces (RIS), or intelligent reconfigurable surfaces (IRS), have recently emerged as a paradigm that can leverage engineered scattering surfaces to transmit and receive information [4]. As a candidate for 6G communications, these surfaces are capable of shaping the radio waves at the electromagnetic level, without the need of radio frequency chains, power amplifiers, or signal processing in general. Specifically, a RIS is a planar array composed

of a large number of passive scattering elements (such as printed dipoles), that induce controlled phase shifts on the incident signal. These phase shifts are independent from the impinging wave, and thus the RIS elements collaborate to modify the propagation of the reflected signal. Eventually, by smartly tuning the phase shift of each element, the reflected signals from different paths can be coherently combined at the desired receiver to improve the quality of the received signal. Accordingly, the RIS can maneuver the propagation environment to boost coverage over the area of interest and avoid blockages.

Although incorporating RIS in wireless systems entails challenging optimization problems, its usage has shown real potential in enhancing point-to-point communications, as well as uplink and downlink multi-user schemes [5]. Within this framework, recent works on RIS-aided wireless systems have predominantly studied the physical layer advantages, while the protocol aspects for their integration have been generally overlooked. In addition, less attention has been paid to control signaling and network stability, defined as the set of users arrival rates that the network can serve within finite time, which are imperative for their operation. For instance, the authors in [6] conceived a simple random access algorithm for RIS-assisted communications, and [7] presented a next generation multiple access (NGMA) scheme with RIS. Moreover, [8] tackled the problem of non-orthogonal multiple access (NOMA) with RIS, and [9] proposed a resource allocation scheme with rate splitting multiple access (RSMA). On the other hand, [10] studied a RIS-aided cell-free MIMO system where distributed access points (APs) in the coverage area cooperate via a backhaul unit to serve the users. This architecture alleviates the intercell interference that characterizes mMIMO [11], and will be used as the physical layer in this work. Furthermore, [12] considers a RIS-assisted cell free massive MIMO scheme with random phase shifts at the RIS and conjugate beamforming at the massive base station (BS) antennas. A closed-form expression of the achievable rate is obtained in [12] and a gain in terms of system coverage and user rate is shown. The aforementioned works focused on the physical layer without considering the impact of dynamic traffic.

Contrary to the previous studies that consider a fixed set of users in the system, we focus in this paper on a more

realistic scenario where users dynamically connect to the network, exchange bursts of information and then leave. We first rigorously describe the physical layer of the communication and the traffic/flow level, where flows represent file transfers. The primary difficulty of this problem is twofold: firstly the presence of the RIS that involves complex analytical forms for the channel modelling, and secondly the dynamic nature of the traffic and the interference between a variable number of users.

In the context of dynamic arrivals departures of users, the goal is to ensure that the network is stable [13]. Network stability implies that all files/users will be served in a finite time. Network stability with dynamic population has been considered in [13] to deal with power control in massive MIMO. In this paper, we consider a different problem of phase shifts in RIS-assisted cell-free MIMO. Instead of considering a sum rate maximization, we show that achieving network stability requires to solve a phase shift framework that depends on the current flows intensity and SINR (Signal to Interference and Noise Ratio) of the users. Typically, globally optimal phase shift solutions cannot be obtained for RIS-related problems due to their non-convexity. We show that a low complexity solution of our proposed framework achieves a guaranteed fraction $\geq 78.5\%$ of the network stability region.

To the best of our knowledge, this is the first work that considers a RIS-assisted wireless environment with dynamic arrival and departures of the users. The remainder of this paper is organized as follows. In section II, the system model is provided with the necessary definitions of stability. The targeted phase shift design problem is then inspected in section III, and the stability analysis is presented in section IV. Numerically evaluated results are given in section V, while section VI concludes the paper.

II. SYSTEM MODEL

A. CHANNEL MODEL

We consider the uplink of a RIS-aided cell-free MIMO system illustrated in Figure 1, where N access points (APs) equipped with a single antenna each, serve K single antenna users who transmit their signals simultaneously on the same time-frequency resource. All APs are linked to a central processing unit (CPU) via a backhaul network. The communication is assisted by an RIS comprising of M reflecting elements. Typically, the number of RIS engineered elements M is very large. We focus on the scenario where the direct channels between the users and the APs are blocked, and the communication is ensured only by the RIS, that can modify the phases of incident signals. These phase shifts introduced by the RIS are adjusted adaptively by a controller linked to the CPU.

We assume a block fading model where the channel realizations are generated randomly and are independent between blocks. The channels between user $k = 1, \dots, K$ and the RIS, and the RIS and AP $n = 1, \dots, N$ are respectively denoted by $\mathbf{g}_k \in \mathbb{C}^{M \times 1}$ and $\mathbf{h}_n \in \mathbb{C}^{M \times 1}$, and are modeled as ergodic processes with independent realizations $\mathbf{g}_k \sim \mathcal{CN}(\mathbf{0}_{M \times 1}, \bar{\mathbf{R}}_k)$ and $\mathbf{h}_n \sim \mathcal{CN}(\mathbf{0}_{M \times 1}, \tilde{\mathbf{R}}_n)$, where $\bar{\mathbf{R}}_k, \tilde{\mathbf{R}}_n \in \mathbb{C}^{M \times M}$

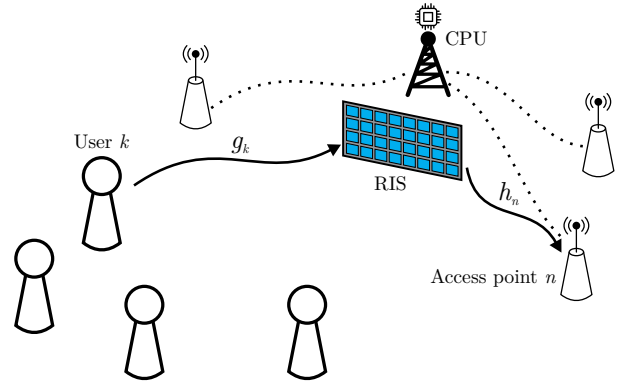


Fig. 1. System Model

are deterministic positive semi-definite covariance matrices that describe the spatial correlation between the channels of the RIS elements. Further, we can write $\bar{\mathbf{R}}_k = \bar{\alpha}_k \mathbf{R}_r$ and $\tilde{\mathbf{R}}_n = \tilde{\alpha}_n \mathbf{R}_t$, with $\bar{\alpha}_k, \tilde{\alpha}_n \in \mathbb{C}$ being the the large-scale fading coefficients, and $\mathbf{R}_r, \mathbf{R}_t$ being the RIS receive and transmit correlation matrices respectively. These matrices can follow a general model that depends on the size, distance and layout of RIS scattering elements, and the propagation environment. For example, a popular model for such planar arrays is the Kronecker model where the correlation matrix is Hermitian Toeplitz with exponential entries $\rho^{|j-i|}$ at row i and column j , if $j \geq i$, where $\rho \in \mathbb{C}$ is the correlation coefficient that satisfies $|\rho| \leq 1$. For the case of isotropic scattering in front of the RIS, the correlation matrix can be explicitly obtained from [14, Proposition 1]. We assume for the rest of this paper, that the transmit and receive correlation matrices are not equal, and the only technical assumption is that their diagonal elements are equal to unity due to power normalization.

The cascaded channel between user k and AP n is then written:

$$u_{n,k} = \mathbf{h}_n^H \Theta \mathbf{g}_k \quad (1)$$

where $\Theta = \text{diag}(\phi)$ is the RIS reflection matrix, with $\phi = [\phi_1, \dots, \phi_M]^T$, $\phi_m = e^{j\theta_m}$ and $\theta = [\theta_1, \dots, \theta_M]^T \in [0, 2\pi]^M$ are the phase shifts of the M elements. We define the aggregated channel from user k to the APs as $\mathbf{u}_k = [u_{1,k}, \dots, u_{N,k}]^T$, where $u_{n,k} = \sum_{m=1}^M h_{nm} g_{km} e^{j\theta_m}$ is the virtual link between the k^{th} user and the n^{th} AP.

Similar models have been studied for massive MIMO systems in [15], and for cell-free MIMO in [10]. For instance, the second moment of the aggregated channel can be directly obtained as:

$$\begin{aligned} \mathbb{E} [|u_{n,k}|^2] &= \mathbb{E} [|\mathbf{h}_n^H \Theta \mathbf{g}_k|^2] \\ &= \mathbb{E} [\text{tr} (\mathbf{h}_n^H \Theta \mathbf{g}_k \mathbf{g}_k^H \Theta^H \mathbf{h}_n)] \\ &= \text{tr} (\Theta^H \mathbb{E} [\mathbf{h}_n \mathbf{h}_n^H] \Theta \mathbb{E} [\mathbf{g}_k \mathbf{g}_k^H]) \\ &= \text{tr} (\Theta^H \tilde{\mathbf{R}}_n \Theta \bar{\mathbf{R}}_k). \end{aligned} \quad (2)$$

We can also see that the channels between two different users and two different APs are mutually independent, $\forall n \neq n', k \neq k', \mathbb{E} [u_{n,k} u_{n',k'}^*] = \mathbb{E} [u_{n,k}] \mathbb{E} [u_{n',k'}^*] =$

0. Moreover, the channels between a user and two different APs are uncorrelated, $\forall n \neq n', \mathbb{E} [u_{n,k} u_{n',k}^*] = \mathbb{E} [(\mathbf{h}_n^H \Theta \mathbf{g}_k) (\mathbf{h}_{n'}^H \Theta \mathbf{g}_k)^*] = 0$, and the channels between two different users and the same AP are also uncorrelated, $\forall k \neq k', \mathbb{E} [u_{n,k} u_{n,k'}^*] = \mathbb{E} [(\mathbf{h}_n^H \Theta \mathbf{g}_k) (\mathbf{h}_n^H \Theta \mathbf{g}_{k'})^*] = 0$. Finally, we define the aggregated channel covariance matrix $\mathbf{Q}_k = \mathbb{E} [\mathbf{u}_k \mathbf{u}_k^H] = \bar{\alpha}_k \text{tr} (\Theta^H \mathbf{R}_t \Theta \mathbf{R}_r) \text{diag} (\tilde{\alpha}_1, \dots, \tilde{\alpha}_N)$.

B. UPLINK TRANSMISSION

In a simultaneous manner, the K users transmit their signals to the N APs, that know an estimate $\hat{u}_{n,k}$ of their channels, computed during the training phase. The baseband received signal at AP n is:

$$y_n = \sum_{k=1}^K u_{n,k} s_k + n_n \quad (3)$$

where the additive noise at the n^{th} AP $n_n \sim \mathcal{CN}(0, \sigma^2)$ and the uplink transmitted symbol $s_k \in \mathbb{C}$ satisfies $\mathbb{E} [|s_k|^2] = P_k$, with $P_k > 0$ being the transmit power budget of user k .

For data detection of the k^{th} symbol, the n^{th} AP multiplies the received signal y_n with the conjugate of its locally obtained channel estimate. The acquired terms are then sent to the CPU via the backhaul network. Therefore, the decision statistic for user k 's symbol s_k reads:

$$r_k = \sum_{n=1}^N \hat{u}_{n,k}^* y_n = \sum_{n=1}^N \sum_{j=1}^K \hat{u}_{n,k}^* u_{n,j} s_j + \sum_{n=1}^N \hat{u}_{n,k}^* n_n. \quad (4)$$

In the following, to maintain analytical tractability, we assume that all users employ mutually orthogonal reverse link pilot sequences. Accordingly, channel estimation error can be neglected when the number of RIS elements M is large, as shown in [16]. Hence, $\hat{u}_{n,k} = u_{n,k}$.

By utilizing the use-and-then-forget bounding technique [17, Theorem 4.4] and the received signal expression in (4), we can show that an achievable uplink rate expression for user k is $\log(1 + \text{SINR}_k)$, where the effective uplink SINR is:

$$\text{SINR}_k = \frac{|\text{DS}_k|^2 P_k}{\sum_{\substack{j=1 \\ j \neq k}}^K \mathbb{E} [|\text{UI}_{j,k}|^2] P_j + \mathbb{E} [|\text{BU}_k|^2] P_k + \mathbb{E} [|\text{NO}_k|^2]} \quad (5)$$

where we have

$$|\text{DS}_k|^2 = \left| \mathbb{E} \left[\sum_{n=1}^N \hat{u}_{n,k}^* u_{n,k} \right] \right|^2 = \left| \mathbb{E} [\mathbf{u}_k^H \mathbf{u}_k] \right|^2 = (\text{tr} (\mathbf{Q}_k))^2 \quad (6)$$

$$\begin{aligned} \mathbb{E} [|\text{UI}_{j,k}|^2] &= \mathbb{E} \left[\left| \sum_{n=1}^N \hat{u}_{n,k}^* u_{n,j} \right|^2 \right] = \mathbb{E} [|\mathbf{u}_k^H \mathbf{u}_j|^2] \\ &= \text{tr} (\mathbf{Q}_k \mathbf{Q}_j) \end{aligned} \quad (7)$$

$$\mathbb{E} [|\text{NO}_k|^2] = \mathbb{E} \left[\left| \sum_{n=1}^N \hat{u}_{n,k}^* n_n \right|^2 \right] = \mathbb{E} [|\mathbf{u}_k^H \mathbf{n}|^2] = \sigma^2 \text{tr} (\mathbf{Q}_k) \quad (8)$$

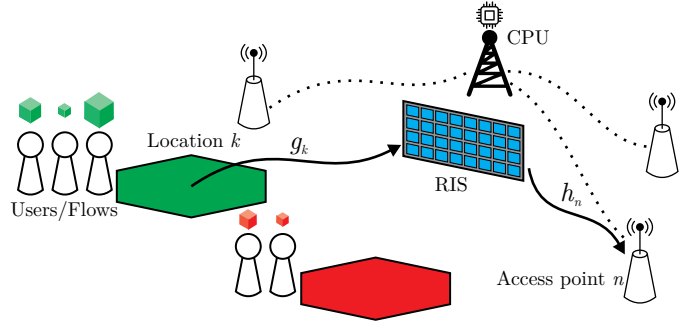


Fig. 2. Flows Arrival Model

$$\begin{aligned} \mathbb{E} [|\text{BU}_k|^2] &= \mathbb{E} \left[\left| \sum_{n=1}^N \hat{u}_{n,k}^* u_{n,k} - \mathbb{E} \left[\sum_{n=1}^N \hat{u}_{n,k}^* u_{n,k} \right] \right|^2 \right] \\ &= \mathbb{V} [\mathbf{u}_k^H \mathbf{u}_k] = \text{tr} (\mathbf{Q}_k^2) \end{aligned} \quad (9)$$

where the final equality follows from [17, Lemma B.14], because the aggregated channels can be approximated by Gaussian distributions when M is large as shown in [16]. These variables represent the strength of the desired signal (DS_k), the beamforming gain uncertainty (BU_k), the interference caused by user j on user k ($\text{UI}_{j,k}$) and the power of additive noise (NO_k). After some algebraic manipulations, we simplify the SINR expression to:

$$\text{SINR}_k = \frac{\bar{\alpha}_k^2 \left(\sum_{n=1}^N \tilde{\alpha}_n \right)^2 \eta P_k}{\sum_{j=1}^K \bar{\alpha}_k \bar{\alpha}_j \left(\sum_{n=1}^N \tilde{\alpha}_n^2 \right) \eta P_j + \sigma^2 \bar{\alpha}_k \left(\sum_{n=1}^N \tilde{\alpha}_n \right)} \quad (10)$$

where $\eta = \text{tr} (\Theta^H \mathbf{R}_t \Theta \mathbf{R}_r)$.

C. USERS / FLOWS ARRIVAL MODEL

All previous works on RIS-aided systems make the assumption that the users are static in the network, in the sense that a fixed number of devices constantly communicate with the BS or the APs. Nevertheless, in real settings, users join the network dynamically, exchange bursts of data with the APs, and leave once they are served. Subsequently, we adopt the model used in [13] for power control in massive MIMO networks, and consider this dynamic user population around the RIS.

Specifically, we consider a finite, but possibly large, number of locations in the network in the vicinity of the RIS. Accordingly, we use K to denote the number of locations instead of users. Let $X_k(t)$ represent the number of users at location k at time t . Each user has one flow to be served, where a flow depicts a file that the user would like to convey to the APs. Thus, the words ‘flow’ and ‘user’ indicate a certain file transfer, and will be interchanged for the rest of this paper. Note that a similar model can be used for the downlink. Also, one can notice that a model where each user has multiple flows is a simple extension to this case. The arrival of the flows at location k is modeled as a Poisson process with rate λ_k . These rates represent the average number of users arriving to each location. The size of the files to be transmitted is

an exponentially distributed random variable S_k at location k with mean $\mathbb{E}[S_k]$. The SINR serving the flow at location k is obtained from (10). Figure 2 displays the considered flows arrival model.

We consider distinct time-scales for the physical layer and the flow level, and we use the time index t to refer to the time at the level of flows. In practice, multiple physical layer timeslots occur between times t and $t + 1$. In the rest of this paper, we will suppress the use of the time index when ambiguity is unlikely.

Next, we define the network stability to be used in the stability analysis.

Definition 1 (Strong Stability [18]). The network is said to be stable if $\limsup_{T \rightarrow \infty} \frac{1}{T} \sum_{t=0}^{T-1} \sum_{k=1}^K \mathbb{E}[X_k(t)] < \infty$

In simple terms, based on this stability definition, if the network is stable then all arriving users are expected to transmit their files in finite time. We let $\boldsymbol{\lambda} = [\lambda_1, \dots, \lambda_K]^T$ denote the vector of user arrival rates. We can now present the definition of a stability region.

Definition 2. The stability region is the set of all mean arrival rate vectors for which there exists a RIS configuration that makes the network stable.

We are now interested in finding a RIS configuration that stabilizes the network whenever possible.

III. RIS PHASE SHIFTS DESIGN

First, we formulate the problem we are interested in solving. Let $\boldsymbol{\Lambda}^{\max}$ be the stability region under RIS configurations. Our target is then:

$$\begin{aligned} \text{Choose } & \boldsymbol{\theta} \in [0, 2\pi]^M \\ \text{such that } & \forall \boldsymbol{\lambda} \in \boldsymbol{\Lambda}^{\max}, \text{ the network is stable.} \end{aligned}$$

Note that the flows' arrival rates λ_k might not be known a priori at the CPU; and hence, the network must be stabilized only by modifying the RIS phase shifts for any arrival rates lying inside the stability region. To accomplish this, we consider the following optimization problem:

$$\begin{aligned} \text{(P1) } & \underset{\boldsymbol{\theta}}{\text{maximize}} & f(\boldsymbol{\theta}) &= \sum_{k=1}^K X_k U_k(\boldsymbol{\theta}) \\ & \text{subject to} & & 0 \leq \theta_i \leq 2\pi \quad i = 1, \dots, M \end{aligned}$$

where we choose the utility functions: $U_k(\boldsymbol{\theta}) = \log(\text{SINR}_k)$ ¹. This choice is motivated by the concavity of the equivalent utility functions with respect to the allocated rates [13]. This asset will be discussed in the next section.

Remark 1. We strongly emphasize that we do not make any kind of approximations in (P1), such as $\log(1 + \text{SINR}) \approx \log(\text{SINR})$ for high SINR values. The objective function can be seen as a sum of each location's utility functions, selected as $\log(\text{SINR}_k)$, weighted by the traffic volume at each location X_k . Regardless, the rate is still equal to $\log(1 + \text{SINR})$.

¹Throughout this paper, we use $\log(\cdot)$ as the natural logarithm function for simplicity, even in the bitrate expression. The analysis remains true for any other base, since all logarithms are equal up to a scaling factor.

Informally, (P1) can be seen as a variation to the proportional fairness problem but at the SINR level.

Solving this optimization problem is challenging, because of the intricate form of its objective function. To mitigate this difficulty, we start by showing that the objective function $f(\boldsymbol{\theta})$ is increasing in η :

$$\begin{aligned} \frac{\partial f(\boldsymbol{\theta})}{\partial \eta} &= \sum_{k=1}^K X_k \times \\ & \frac{\sigma^2 \bar{\alpha}_k \left(\sum_{n=1}^N \tilde{\alpha}_n \right)}{\eta \left(\sigma^2 \bar{\alpha}_k \left(\sum_{n=1}^N \tilde{\alpha}_n \right) + \sum_{j=1}^K \bar{\alpha}_k \bar{\alpha}_j \left(\sum_{n=1}^N \tilde{\alpha}_n^2 \right) \eta P_j \right)} > 0. \end{aligned} \quad (11)$$

On the other hand, notice that $\eta = \text{tr}(\boldsymbol{\Theta}^H \mathbf{R}_t \boldsymbol{\Theta} \mathbf{R}_r) = \boldsymbol{\phi}^H \mathbf{R} \boldsymbol{\phi}$, where $\mathbf{R} = \mathbf{R}_t \odot \mathbf{R}_r^T$ is positive semi-definite by virtue of the Schur product theorem [20]. Thus, (P1) is equivalent to:

$$\begin{aligned} \text{(P2) } & \underset{\boldsymbol{\phi}}{\text{maximize}} & \boldsymbol{\phi}^H \mathbf{R} \boldsymbol{\phi} \\ & \text{subject to} & |\phi_i| = 1 \quad i = 1, \dots, M \end{aligned}$$

(P2) is a complex quadratic optimization problem, that is in the class of NP-hard problems; and therefore a globally optimal solution cannot be obtained in polynomial time. However, we know in this case, that applying the semi-definite relaxation (SDR) technique reported in [21] can bound the error committed while approximating the solution. As such, the following semi-definite program (SDP) provides a relaxation for (P2):

$$\begin{aligned} \text{(P3) } & \underset{\boldsymbol{\Phi}}{\text{maximize}} & \text{tr}(\mathbf{R} \boldsymbol{\Phi}) \\ & \text{subject to} & \boldsymbol{\Phi} \succeq \mathbf{0}, \boldsymbol{\Phi}_{i,i} = 1 \quad i = 1, \dots, M \end{aligned}$$

where $\boldsymbol{\Phi} = \boldsymbol{\phi} \boldsymbol{\phi}^H$. (P3) is standard convex optimization problem that can be optimally solved by invoking interior-point based solvers, such as CVX [22]. If the obtained solution $\boldsymbol{\Phi}^*$ is rank-one, then it is also the optimal solution to (P2). But since this is not generally the case, we construct a rank-one solution to (P2) from $\boldsymbol{\Phi}^*$ using Gaussian randomization as follows. We first compute the eigenvalue decomposition $\boldsymbol{\Phi}^* = \mathbf{U} \boldsymbol{\Sigma} \mathbf{U}^H$, where \mathbf{U} and $\boldsymbol{\Sigma}$ are a unitary and a diagonal matrix respectively. Then we obtain a sub-optimal solution to (P2) as $\bar{\boldsymbol{\phi}} = \mathbf{U} \boldsymbol{\Sigma}^{1/2} \mathbf{r}$ where $\mathbf{r} \in \mathbb{C}^{M \times 1}$ is a random vector generated according to $\mathbf{r} \sim \mathcal{CN}(\mathbf{0}_{M \times 1}, \mathbf{I}_M)$. By drawing independent random vectors \mathbf{r} , the objective function of (P2) is approximated by the maximum one attained by the corresponding $\bar{\boldsymbol{\phi}}$. We finally recover a suboptimal solution to (P2) as a vector $\boldsymbol{\phi}$ with elements $\phi_i = e^{j \arg(\bar{\phi}_i)}$, $1 \leq i \leq M$. It has been shown in [21], [23] that such techniques with a sufficiently large number of randomizations, guarantee a $\frac{\pi}{4}$ -approximation to (P2), in following sense:

$$\frac{\pi}{4} \eta^{\text{opt}} \leq \eta^{\text{sub}} \leq \eta^{\text{opt}} \quad \text{or} \quad \frac{\pi}{4} \leq \gamma = \frac{\eta^{\text{sub}}}{\eta^{\text{opt}}} \leq 1 \quad (12)$$

where η^{opt} and η^{sub} are the optimal and approximate solutions of (P2), and γ is the approximation accuracy.

²This is a direct application of [19, Theorem 1.11].

It is worth noting that a similar method can be applied to solve the same problem in the case the RIS phase shifts can only take a finite number of discrete values. In such scenarios, $\phi \in \mathcal{V}_L = \{1, \omega, \dots, \omega^{L-1}\}$, where ω is the principal L^{th} root of unity and L is the number of phase shift levels. The minimum approximation accuracy becomes $\frac{(L \sin(\frac{\pi}{L}))^2}{4\pi}$.

Due to the complexity of the channel induced by the presence of a RIS in the network, (P1) cannot be optimally solved. This will affect the stability analysis which we will discuss later. Yet, we could at least bound the error carried out with the aforementioned solution. This error will however decrease the stability region insured by solving (P1) to a smaller region. Nonetheless, we can still acquire the closed-form solution to (P1) in the special case where the transmit and receive correlation matrices are equal.

Corollary 1. If the transmit and receive correlation matrices are equal $\mathbf{R}_t = \mathbf{R}_r$, any equal RIS phase shift configuration ($\theta_1 = \theta_2 = \dots = \theta_M$) is the optimal maximizer of (P1).

Proof. Notice that since \mathbf{R}_t and \mathbf{R}_r are Hermitian, $\mathbf{R} = \mathbf{R}_t \odot \mathbf{R}_r^\dagger$ is symmetric, and has real non negative elements. Then,

$$\begin{aligned} \eta &= \text{tr}(\Theta^H \mathbf{R}_t \Theta \mathbf{R}_r) = \sum_{m=1}^M \sum_{n=1}^M [\mathbf{R}]_{m,n} e^{j\theta_n - j\theta_m} \\ &= \sum_{m=1}^M \sum_{n=1}^M [\mathbf{R}]_{m,n} \cos(\theta_n - \theta_m) \end{aligned} \quad (13)$$

which is maximized for any equal phase shifts configuration. ■

When the correlation matrices are equal, Corollary 1 provides a simple yet effective option for the phase shifts design, and optimally solves the desired problem.

IV. STABILITY ANALYSIS OF THE NETWORK

In this part, we will show that the RIS configuration presented in the previous section, i.e. the one that solves (P1), guarantees the network stability for any flow arrival rates inside the stability region Λ^{\max} when (P1) is solved with no optimality gap, and for all flow arrival rates that are within a factor proportional to the optimality gap otherwise. To do so, we utilize fluid limit analysis to demonstrate the stability. In other terms, for the stochastic process $\mathbf{X}(t) = [X_1(t), \dots, X_K(t)]^\top$ that portrays the flows' volumes, we introduce a deterministic process $\mathbf{Y}(t)$ that approximates the evolution of \mathbf{X} subject to a certain limiting criteria. It is known that if the fluid limit associated to a stochastic process reaches zero in finite time, then the process itself is stable. Furthermore, to show that \mathbf{Y} is stable, it is sufficient to prove that its corresponding Lyapunov function exhibits negative drift under the selected RIS configuration [24], [25].

Recall that the users' arrivals follow a Poisson distribution with mean λ_k at location k . We suppose that when a new user joins the network, he directly starts a connection with the APs and transmits a file having an average size of $\mathbb{E}[S_k] = 1 \forall k$. It will then be straightforward to extend this situation to different file size means and renewal arrival processes. In this context,

it is clear that \mathbf{X} is a Markov process that has the following evolution at each timeslot t , and at each location k :

$$\begin{aligned} X_k &\longrightarrow X_k + 1 && \text{at rate} && \lambda_k \\ X_k &\longrightarrow X_k - 1 && \text{at rate} && R_k \end{aligned}$$

where R_k is the physical layer rate allocated to location k between time instants t and $t + 1$. This rate is expressed as $R_k = \log(1 + \text{SINR}_k)$, where the SINR at each location is given by (10).

After introducing all the necessary ingredients, we now state the main result of this paper.

Theorem 1. By choosing the RIS phase shifts that solve (P1), the network is stable for any user arrival rate vector $\gamma \boldsymbol{\lambda}$, where $\boldsymbol{\lambda} \in \Lambda^{\max}$ and $\gamma \in [\frac{\pi}{4}, 1]$ is the approximation accuracy of (P2).

The aforementioned theorem implies that our proposed solution allows achieving a guaranteed fraction higher than $\pi/4$ (i.e. higher than 78.5%) of the stability region.

Proof. Before proving the theorem, we provide a useful lemma for the demonstration.

Lemma 1. $\forall \gamma \in (0, 1], \forall x > 0$, $\log(1 + \gamma x) \geq \gamma \log(1 + x)$, with equality when $\gamma = 1$.

Proof. When $\gamma = 1$ the equality is obvious. Otherwise, $\forall \gamma \in (0, 1), \forall x > 0$, the proof follows by composing both sides of Bernoulli's inequality [26] $(1 + x)^\gamma < 1 + \gamma x$ with the increasing function $x \mapsto \log(x)$. ■

The proof consists of studying the fluid system obtained when the initial number of flows grows to infinity. Specifically, we consider the set of fluid limits defined by:

$$Y_k(t) = \lim_{\beta \rightarrow \infty} \frac{X_k(\beta t)}{\beta} \quad \text{with} \quad \sum_{k=1}^K X_k(0) = \beta.$$

Notice that if the limit exists, $\sum_{k=1}^K Y_k(0) = 1$. Given this initial distribution of the fluid system $\mathbf{Y}(0)$, the evolution of $\mathbf{Y}(t)$ is uniquely defined by the following set of differential equations, given by the strong law of large numbers:

$$\frac{d}{dt} Y_k(t) = \lambda_k - R_k \quad \text{for all } k, t \text{ such that } Y_k(t) > 0. \quad (14)$$

Now, we define $\mathbf{R} = [R_1, \dots, R_K]^\top$ as a vector containing the allocated rates at each location. Recall that the rate is calculated by $R_k = \log(1 + \text{SINR}_k)$. Conversely we can write $\log(\text{SINR}_k) = \log(e^{R_k} - 1)$. Then, (P1) is equivalent to the following optimization problem:

$$\begin{aligned} \text{(P4)} \quad & \underset{\mathbf{R}}{\text{maximize}} && \sum_{k=1}^K Y_k \log(e^{R_k} - 1) \\ & \text{subject to} && 0 \leq f_i(\mathbf{R}) \leq 2\pi, \quad i = 1, \dots, M \end{aligned}$$

where \mathbf{X} is interchanged with its limit \mathbf{Y} , and the constraint functions $f_i(\mathbf{R})$ are the equivalent of the phase shift constraints on $\boldsymbol{\theta}$. Let $\text{SINR}_k(\eta)$ denote the SINR value at location

k for a given value of η . Since $\text{SINR}_k(\eta)$ increases with η , we have from (12):

$$\gamma \text{SINR}_k(\eta^{\text{opt}}) \stackrel{(a)}{\leq} \text{SINR}_k(\gamma \eta^{\text{opt}}) \leq \text{SINR}_k(\eta^{\text{sub}}) \leq \text{SINR}_k(\eta^{\text{opt}}) \quad (15)$$

where (a) is a straightforward bound due to $0 < \gamma \leq 1$. Moreover, for any $x > 0$ the function $x \mapsto \log(1+x)$ is increasing and thus,

$$\begin{aligned} \gamma \log(1 + \text{SINR}_k(\eta^{\text{opt}})) &\stackrel{(b)}{\leq} \log(1 + \gamma \text{SINR}_k(\eta^{\text{opt}})) \\ &\leq \underbrace{\log(1 + \text{SINR}_k(\eta^{\text{sub}}))}_{R_k^{\text{sub}}} \leq \underbrace{\log(1 + \text{SINR}_k(\eta^{\text{opt}}))}_{R_k^{\text{opt}}} \end{aligned} \quad (16)$$

where (b) is a direct application of Lemma 1. We define $\mathbf{R}^{\text{sub}} = [R_1^{\text{sub}}, \dots, R_K^{\text{sub}}]^\top$ and $\mathbf{R}^{\text{opt}} = [R_1^{\text{opt}}, \dots, R_K^{\text{opt}}]^\top$. Due to the equivalence between (P1) and (P4), \mathbf{R}^{sub} and \mathbf{R}^{opt} are, respectively, the approximate and optimal solution to (P4). The series of inequalities in (15) and (16) mean that if γ is the approximation accuracy of (P2) in the sense of (12), then γ is also an approximation accuracy in the same sense for the SINR and the rate at all locations. On the other hand, the objective function of (P4) is the sum of strictly concave functions $\log(e^{R_k} - 1)$ with respect to R_k . These concave functions are always upper bounded by the first order of their Taylor expansion. Particularly, we have:

$$\log(e^{R_k^{\text{sub}}} - 1) \leq \log(e^{\gamma \lambda_k} - 1) + \frac{e^{\gamma \lambda_k}}{e^{\gamma \lambda_k} - 1} (R_k^{\text{sub}} - \gamma \lambda_k) \quad (17)$$

for any arrival rate $\gamma \lambda_k$. Furthermore, for $x > 0$, the function $x \mapsto \log(e^x - 1)$ is strictly increasing. This implies that for any arrival rate vector $\boldsymbol{\lambda}$ inside the stability region, we can write:

$$\sum_{k=1}^K Y_k \log(e^{R_k^{\text{sub}}} - 1) \geq \sum_{k=1}^K Y_k \log(e^{\gamma \lambda_k} - 1) \quad (18)$$

because at all locations, $R_k^{\text{sub}} > \gamma \lambda_k$ is true for all arrival rate vectors including \mathbf{R}^{opt} . Combining (17) and (18), we obtain the following inequality:

$$\sum_{k=1}^K Y_k \frac{e^{\gamma \lambda_k}}{e^{\gamma \lambda_k} - 1} (\gamma \lambda_k - R_k^{\text{sub}}) \leq 0. \quad (19)$$

We now introduce the quadratic Lyapunov function $\mathcal{L}(\mathbf{Y}(t)) = \sum_{k=1}^K \frac{1}{2} \frac{e^{\gamma \lambda_k + \epsilon}}{e^{\gamma \lambda_k + \epsilon} - 1} Y_k^2(t)$, where for any arrival rate $\gamma \lambda_k$ lying strictly inside the stability region, we select $\epsilon > 0$ such that $\forall k, \gamma \lambda_k + \epsilon$ is inside or on the boundary of the region. We get from (14):

$$\frac{d}{dt} \mathcal{L}(\mathbf{Y}) = \sum_{k=1}^K Y_k \frac{e^{\gamma \lambda_k + \epsilon}}{e^{\gamma \lambda_k + \epsilon} - 1} (\gamma \lambda_k - R_k^{\text{sub}}). \quad (20)$$

Replacing $\gamma \lambda_k$ with $\gamma \lambda_k + \epsilon$ in (19) yields: $\sum_{k=1}^K Y_k \frac{e^{\gamma \lambda_k + \epsilon}}{e^{\gamma \lambda_k + \epsilon} - 1} (\gamma \lambda_k + \epsilon - R_k^{\text{sub}}) \leq 0$. In view of (20), this reads:

$$\frac{d}{dt} \mathcal{L}(\mathbf{Y}) \leq -\epsilon \sum_{k=1}^K Y_k \frac{e^{\gamma \lambda_k + \epsilon}}{e^{\gamma \lambda_k + \epsilon} - 1}. \quad (21)$$

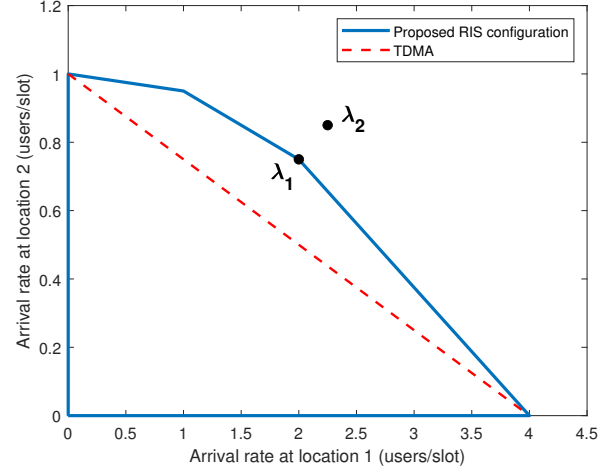


Fig. 3. Simulation Results: Stability Region

By using the the inequality

$$2 \times \mathcal{L}(\mathbf{Y}) = \sum_{k=1}^K \frac{e^{\gamma \lambda_k + \epsilon}}{e^{\gamma \lambda_k + \epsilon} - 1} Y_k^2(t) \leq \left(\sum_{k=1}^K \frac{e^{\gamma \lambda_k + \epsilon}}{e^{\gamma \lambda_k + \epsilon} - 1} Y_k(t) \right)^2,$$

we conclude that there exists a constant $\xi > 0$ such that:

$$\frac{d}{dt} \mathcal{L}(\mathbf{Y}) \leq -\xi \sqrt{\mathcal{L}(\mathbf{Y})} \quad (22)$$

This implies for all $t \geq 0$ such that $\mathcal{L}(\mathbf{Y}(t)) \geq 0$:

$$\mathcal{L}(\mathbf{Y}(t)) \leq \left(\sqrt{\mathcal{L}(\mathbf{Y}(0))} - \frac{\xi}{2} t \right)^2 \quad (23)$$

and also $\sqrt{\mathcal{L}(\mathbf{Y}(t))} \leq \left(\sqrt{\mathcal{L}(\mathbf{Y}(0))} - \frac{\xi}{2} t \right)$ since $\mathcal{L}(\mathbf{Y}(t)) \geq 0$. Therefore, the inequality in (22) means that if there exists some $T > 0$ with $\mathcal{L}(\mathbf{Y}(T)) = 0$, then $\mathcal{L}(\mathbf{Y}(t)) = 0$ for all $t \geq T$. Looking at (23), we select:

$$T = \frac{2}{\xi} \sqrt{\sum_{k=1}^K \frac{1}{2} \frac{e^{\gamma \lambda_k + \epsilon}}{e^{\gamma \lambda_k + \epsilon} - 1}} \quad (24)$$

This implies that for all $t \geq T$, $\mathcal{L}(\mathbf{Y}(t))$ and thus $\mathbf{Y}(t)$ are identically zero, and the system is stable. ■

Before providing our simulation results, we recapitulate the systematic way of obtaining this result. First, we represent the queueing model by a vector $\mathbf{X}(t)$ containing the number of users at each location. Given the arrival model, we obtain the temporal equation describing the evolution of \mathbf{X} . Then, using the law of large numbers, a similar limit equation can be obtained for its fluid limit \mathbf{Y} . Knowing that the allocated rate at each location should be strictly larger than the arrival rate in order to guarantee the stability, we bound the suboptimal rates obtained from (P1) and show that they are optimal in the scaled stability region. Finally, we use the Lyapunov technique to show that \mathbf{Y} reaches zero in finite time for these arrival rates. It is then a direct conclusion that the network is stable.

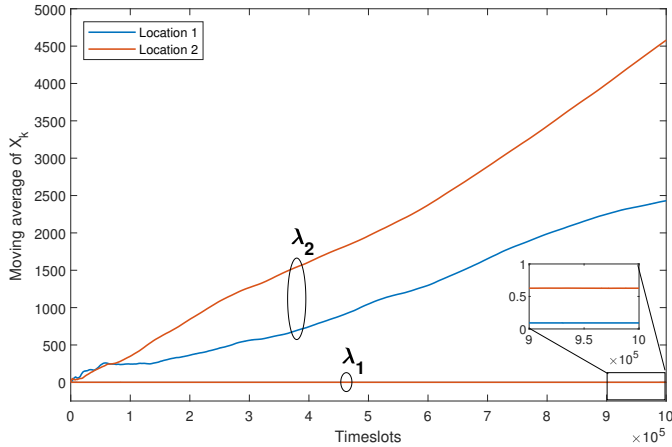


Fig. 4. Simulation Results: Moving average of the number of users for different arrival rates

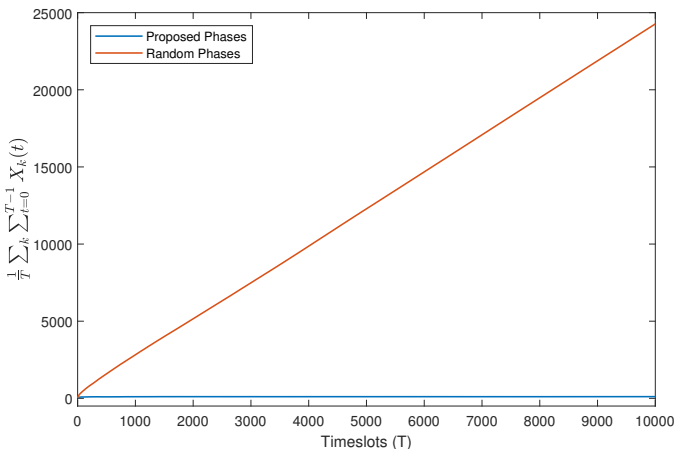


Fig. 5. Simulation Results: Evolution of the stability metric for different phase shift designs. The arrival rate is fixed at 0.1 users/slot at all locations.

V. NUMERICAL RESULTS

In this section, we report some simulation results in order to illustrate the stability of the considered wireless system. We consider a 2×2 km² area with $N = 128$ APs uniformly distributed in the lower left sub-region with coordinates $x, y \in [-0.75, -1]$ and the RIS with $M = 1600$ elements is located at the origin. The bandwidth of the system is 20 MHz and the carrier frequency is 1.9 GHz. The large scale fading coefficients are generated according to the three-slope model in [27, Section VI].

For visual considerations, we start by considering $K = 2$ locations in the upper right region, with both coordinates being 0.25 and 0.75 for each location respectively. The users arrive to each location according to a Poisson process and transmit packets of 1 Mbits with a power budget of 20 dBm. In Figure 3 we compare the network stability region obtained by employing our proposed phase shifts design and the one obtained by using time division multiple access (TDMA) where at each timeslot, the RIS phases are optimized to maximize the SNR of the active user. We notice that the TDMA stability region

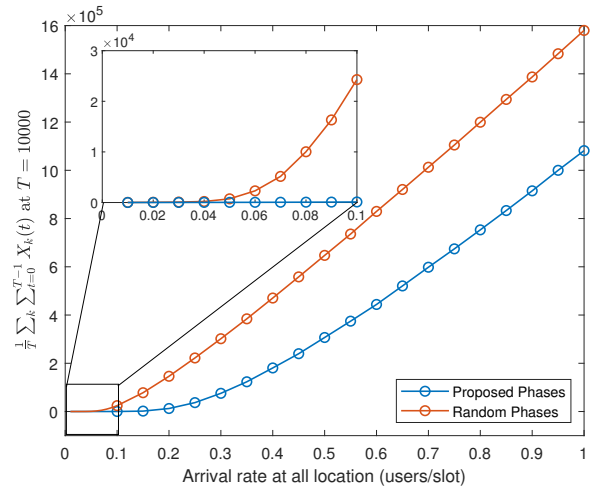


Fig. 6. Simulation Results: Stability metric versus the arrival rate at all locations for different phase shift designs. The metric is calculated at $T=10000$ timeslots.

is contained within the one guaranteed by our proposed RIS configuration. In Figure 4, we show the moving average of the locations' user density. These correspond to two arrival vectors shown as points λ_1 and λ_2 on the stability region in Figure 3. Clearly, under the arrival rates of λ_1 the network is stable since the average traffic converges to a constant; while it is unstable for the arrival rates of λ_2 since this average diverges with time. Thus λ_2 is outside the stability region.

We now consider $K = 400$ locations whose coordinates $x, y \in [0.05, 1]$ form a square mesh in the upper right sub-region. In Figure 5, we compare, for an arrival rate equal to 0.1 users/slot at all locations, the sum over the locations of the moving average of the users density, when using our proposed RIS configuration to the one obtained by drawing each phase uniformly at random from $[0, 2\pi]$ at each timeslot. It is clear that the network is not stable using random RIS phases since the number of flows grows rapidly with time, while this number is bounded when using the proposed phase shifts. In Figure 6, we plot the stability metric computed at $T = 10000$ timeslots versus the arrival rate at all locations, for our proposed RIS phase shifts and the random phases scheme. We first remark the metric varies exponentially with respect to the arrival rate. Secondly, we evince that the network is stable for a wider region of arrival rates when the RIS phases are optimized as we proposed, compared to the case where they are randomly selected, since the stability metric diverges at a prior point in the latter case.

VI. CONCLUSION

In this paper, we studied the stability of a RIS-assisted cell-free MIMO system where the number of users in the network is time-varying. We started by obtaining a closed form physical layer rate expression, and then described the data layer flow arrivals. Next, we proposed an optimization framework for the RIS induced phases. With no power control nor scheduling, we showed that by only optimizing the RIS phases, our proposed

configuration ensures the system's stability inside a scaled version of the stability region. We have also shown that this scaling factor is bounded.

REFERENCES

- [1] T. L. Marzetta, "Noncooperative cellular wireless with unlimited numbers of base station antennas," *IEEE transactions on wireless communications*, vol. 9, no. 11, pp. 3590–3600, 2010.
- [2] S. E. Hajri, M. Assaad, and G. Caire, "Scheduling in massive mimo: User clustering and pilot assignment," in *2016 54th Annual Allerton Conference on Communication, Control, and Computing (Allerton)*. IEEE, 2016, pp. 107–114.
- [3] F. Boccardi, R. W. Heath, A. Lozano, T. L. Marzetta, and P. Popovski, "Five disruptive technology directions for 5g," *IEEE communications magazine*, vol. 52, no. 2, pp. 74–80, 2014.
- [4] C. Liaskos, S. Nie, A. Tsioliaridou, A. Pitsillides, S. Ioannidis, and I. Akyildiz, "A new wireless communication paradigm through software-controlled metasurfaces," *IEEE Communications Magazine*, vol. 56, no. 9, pp. 162–169, 2018.
- [5] Q. Wu and R. Zhang, "Intelligent reflecting surface enhanced wireless network via joint active and passive beamforming," *IEEE Transactions on Wireless Communications*, vol. 18, no. 11, pp. 5394–5409, 2019.
- [6] V. Croisfelt, F. Saggese, I. Leyva-Mayorga, R. Kotaba, G. Gradoni, and P. Popovski, "A random access protocol for ris-aided wireless communications," in *2022 IEEE 23rd International Workshop on Signal Processing Advances in Wireless Communication (SPAWC)*. IEEE, 2022, pp. 1–5.
- [7] X. Cao, B. Yang, C. Huang, G. C. Alexandropoulos, C. Yuen, Z. Han, H. V. Poor, and L. Hanzo, "Massive access of static and mobile users via reconfigurable intelligent surfaces: protocol design and performance analysis," *IEEE Journal on Selected Areas in Communications*, vol. 40, no. 4, pp. 1253–1269, 2022.
- [8] G. Yang, X. Xu, Y.-C. Liang, and M. Di Renzo, "Reconfigurable intelligent surface-assisted non-orthogonal multiple access," *IEEE Transactions on Wireless Communications*, vol. 20, no. 5, pp. 3137–3151, 2021.
- [9] Z. Yang, J. Shi, Z. Li, M. Chen, W. Xu, and M. Shikh-Bahaei, "Energy efficient rate splitting multiple access (rsma) with reconfigurable intelligent surface," in *2020 IEEE International Conference on Communications Workshops (ICC Workshops)*. IEEE, 2020, pp. 1–6.
- [10] T. Van Chien, H. Q. Ngo, S. Chatzinotas, M. Di Renzo, and B. Ottersten, "Reconfigurable intelligent surface-assisted cell-free massive mimo systems over spatially-correlated channels," *IEEE Transactions on Wireless Communications*, vol. 21, no. 7, pp. 5106–5128, 2022.
- [11] J. Denis and M. Assaad, "Improving cell-free massive mimo networks performance: A user scheduling approach," *IEEE Transactions on Wireless Communications*, vol. 20, no. 11, pp. 7360–7374, 2021.
- [12] B. Al-Nahhas, M. Obeed, A. Chaaban, and M. J. Hossain, "Ris-aided cell-free massive mimo: Performance analysis and competitiveness," in *IEEE International Conference on Communications Workshops (ICC Workshops)*. IEEE, 2021, pp. 1–6.
- [13] M. Assaad, S. E. Hajri, T. Bonald, and A. Ephremides, "Power control in massive mimo with dynamic user population," in *2018 IEEE Globecom Workshops (GC Wkshps)*. IEEE, 2018, pp. 1–6.
- [14] E. Björnson and L. Sanguinetti, "Rayleigh fading modeling and channel hardening for reconfigurable intelligent surfaces," *IEEE Wireless Communications Letters*, vol. 10, no. 4, pp. 830–834, 2020.
- [15] T. Van Chien, H. Q. Ngo, S. Chatzinotas, and B. Ottersten, "Reconfigurable intelligent surface-assisted massive mimo: Favorable propagation, channel hardening, and rank deficiency [lecture notes]," *IEEE Signal Processing Magazine*, vol. 39, no. 3, pp. 97–104, 2022.
- [16] Z. Wang, L. Liu, S. Zhang, and S. Cui, "Massive mimo communication with intelligent reflecting surface," *arXiv preprint arXiv:2107.04255*, 2021.
- [17] E. Björnson, J. Hoydis, L. Sanguinetti *et al.*, "Massive mimo networks: Spectral, energy, and hardware efficiency," *Foundations and Trends® in Signal Processing*, vol. 11, no. 3-4, pp. 154–655, 2017.
- [18] M. J. Neely, "Stability and capacity regions or discrete time queueing networks," *arXiv preprint arXiv:1003.3396*, 2010.
- [19] X. Zhang, *Matrix analysis and applications*. Cambridge University Press, 2017.
- [20] J. Schur, "Bemerkungen zur theorie der beschränkten bilinearformen mit unendlich vielen veränderlichen." *Journal für die reine und angewandte Mathematik*, vol. 140, pp. 1–28, 1911. [Online]. Available: <http://eudml.org/doc/149352>
- [21] A. M.-C. So, J. Zhang, and Y. Ye, "On approximating complex quadratic optimization problems via semidefinite programming relaxations," *Mathematical Programming*, vol. 110, no. 1, pp. 93–110, 2007.
- [22] M. Grant and S. Boyd, "Cvx: Matlab software for disciplined convex programming, version 2.1," 2014.
- [23] Z.-Q. Luo, W.-K. Ma, A. M.-C. So, Y. Ye, and S. Zhang, "Semidefinite relaxation of quadratic optimization problems," *IEEE Signal Processing Magazine*, vol. 27, no. 3, pp. 20–34, 2010.
- [24] T. Bonald and L. Massoulié, "Impact of fairness on internet performance," in *Proceedings of the 2001 ACM SIGMETRICS international conference on Measurement and modeling of computer systems*, 2001, pp. 82–91.
- [25] M. Andrews, K. Kumaran, K. Ramanan, A. Stolyar, R. Vijayakumar, and P. Whiting, "Scheduling in a queueing system with asynchronously varying service rates," *Probability in the Engineering and Information Sciences*, vol. 18, no. 2, pp. 191–217, 2004.
- [26] P. S. Bullen, *Handbook of means and their inequalities*. Springer Science & Business Media, 2013, vol. 560.
- [27] H. Q. Ngo, A. Ashikhmin, H. Yang, E. G. Larsson, and T. L. Marzetta, "Cell-free massive mimo versus small cells," *IEEE Transactions on Wireless Communications*, vol. 16, no. 3, pp. 1834–1850, 2017.